Quantitative Assessment of Optical Properties in Healthy Cartilage and Repair Tissue by Optical Coherence Tomography and Histology

Paul Cernohorsky, Sanne M. Jansen, Daniel M. de Bruin, Edwin van der Pol, Cemile D. Savci-Heijink, Simon D. Strackee, Dirk J. Faber, and Ton G. van Leeuwen, *Member, IEEE*

***Abstract*—Quantification of the OCT signal is an important step toward clinical implementation of a diagnostic tool in cartilage imaging. Discrimination of structural cartilage differences in patients with osteoarthritis is critical, yet challenging. This study assesses the variation in the optical attenuation coefficient (μ_{OCT}) between healthy cartilage, repair tissue, bone, and layers within repair tissue in a controlled setting. OCT and histology were used to assess goat talus articular surfaces in which central osteochondral defects were created. Exact matches of OCT and histology were selected for research. μ_{OCT} measurements were taken from healthy cartilage, repair tissue, and bone. Measured μ_{OCT} in healthy cartilage was higher compared to both repair tissue and bone tissue. Two possible mechanisms for the difference in attenuation were investigated. We studied morphological parameters in terms of nucleus count, nucleus size, and inter-nucleus distance. Collagen content in healthy cartilage and repair tissue was assessed using polarization microscopy. Quantitative analysis of the nuclei did not demonstrate a difference in nucleus size and nucleus count between healthy cartilage and repair tissue. In healthy cartilage, cells were spaced farther apart and had a lower variation in local nuclear density compared to the repair tissue. Polarization microscopy suggested higher collagen content in the healthy cartilage compared to the repair tissue. μ_{OCT} measurements can distinguish between healthy cartilage, repair tissue, and bone. Results suggest that cartilage OCT attenuation measurements could be of great impact in clinical diagnostics of osteoarthritis.**

Manuscript received July 29, 2015; revised October 2, 2015; accepted October 20, 2015. P. Cernohorsky and S. M. Jansen contributed equally to this work.

P. Cernohorsky and S. D. Strackee are with the Department of Plastic, Reconstructive, and Hand Surgery, Academic Medical Center, University of Amsterdam, Amsterdam 1012 WX, The Netherlands (e-mail: p.cernohorsky@amc.uva.nl; s.d.strackee@amc.uva.nl).

S. M. Jansen is with the Department of Plastic, Reconstructive, and Hand Surgery, Amsterdam, 1012 WX, The Netherlandsand also with the Department of Biomedical Engineering and Physics, Academic Medical Center, University of Amsterdam, Amsterdam 1012 WX, The Netherlands (e-mail: s.m.jansen@amc.uva.nl).

D. M. de Bruin and D. J. Faber are with the Department of Biomedical Engineering and Physics, Academic Medical Center, University of Amsterdam, Amsterdam 1012 WX, The Netherlands (e-mail: d.m.debruin@amc.uva.nl; d.j.faber@amc.uva.nl).

E. van der Pol is with the Department of Biomedical Engineering & Physics, University of Amsterdam, Amsterdam, 1012 WX, The Netherlands, and also with the Laboratory of Experimental Clinical Chemistry, Academic Medical Center, University of Amsterdam, Amsterdam 1012 WX, The Netherlands (e-mail: e.vanderpol@amc.uva.nl).

C. D. Savci-Heijink is with the Department of Pathology, Academic Medical Center, University of Amsterdam, Amsterdam 1012 WX, The Netherlands (e-mail: c.d.savciheijink@amc.uva.nl).

T. G. van Leeuwen is with the Department of Biomedical Engineering and Physics, Academic Medical CenterUniversity of Amsterdam, Amsterdam 1012 WX, The Netherlands (e-mail: t.g.vanleeuwen@amc.uva.nl).

Color versions of one or more of the figures in this paper are available online at http://ieeexplore.ieee.org.

Digital Object Identifier 10.1109/JSTQE.2015.2499958

***Index Terms*—Anatomical structure, attenuation measurement, biomedical optical imaging, medical diagnostic imaging, Optical coherence tomography (OCT).**

I. Introduction

In DEGENERATIVE joint disease, often a discrepancy exists between clinical symptoms and changes as seen on imaging studies. Accurate imaging of the thin layers of articular cartilage lining small joints may overcome this problem. However, conventional clinical imaging techniques are unable to accurately depict the subtle early changes in articular cartilage associated with degenerative joint disease, such as osteoarthritis (OA).

Given a typical resolution of $\sim$15 μm with 2–3 mm imaging depth, Optical Coherence Tomography (OCT) is a promising technique in imaging of thin layers of articular cartilage. OCT has shown to be of use in *in vivo* detection of cartilage pathology associated with OA in larger joints like the knee [1]–[4]. Recent developments in OCT design have yielded commercially available systems utilizing a thin fiber-optic probe [1]–[4], paving the way for application of cartilage OCT in small joints. To enhance the value of OCT in clinical diagnostics, quantification of cartilage OCT data is an important step. Various methods of quantification of the OCT signal include layer thickness and surface fibrillation [5]–[9]. A measure for local tissue composition is provided by the optical attenuation coefficient (μ_{OCT}), which describes the decay in OCT signal amplitude as a function of imaging depth [10]–[14].

In a previous study [15] we suggested a role for the attenuation coefficient in quantitative imaging of articular cartilage. The relation between differences in μ_{OCT} from healthy and damaged articular cartilage on one hand and morphological changes on the other hand, is hitherto unknown. It is thought that cellular components such as nuclei and mitochondria are mainly responsible for scattering properties in highly reflective tissue [16], [17]. Since collagen is an important component in cartilage tissue, the collagen content and fiber orientation may also govern light scattering in cartilage tissue.

The aim of this study is to investigate light attenuation in articular cartilage, relating μ_{OCT} to morphological differences in healthy cartilage, repair tissue and bone, enhancing apprehension of the OCT signal in cartilage pathology. In order to elucidate the origin of the differences in light scattering in healthy cartilage and repair tissue, quantitative histological parameters in terms of *nuclei per mm^2, nucleus size and mean nearest neighbor nucleus distance* were performed from registered pathology

slides. Moreover, qualitative collagen fiber content was imaged using polarization microscopy.

II. Methods

A. Samples

This study protocol was approved by the Animal Welfare Committee of the Academic Medical Center, University of Amsterdam (ORCA102287). Sample preparation was performed as described earlier [18]. In short, healing of the talar articular surface from ten Dutch milk goats (Capra hircus sana) of the same age (4 years) was investigated. Thereto, an osteochondral defect of 6 mm diameter was drilled until 3 mm of depth, perpendicular to the center of the talus surface, under continuous lavage with 0.9% NaCl. After 24 weeks of follow-up and spontaneous healing of the tali, the goats were sacrificed. All tali were cut into 20×20 mm blocks around the osteochondral defect and the anterior saw plane was marked. Samples were fixed in 4% formaldehyde and dehydrated in ethanol.

B. Optical Coherence Tomography

OCT imaging was performed using a 50 kHz Santec IVS-2000 mobile OCT platform (Santec, Corporation, Aichi, Japan) with a high-speed scanning laser light source (HSL-2000) operating at a central wavelength of 1300 nm with a bandwidth of 120 nm. Images were captured at a rate of 75 frames per second, with a lateral resolution of $\sim$20 μm. Cartilage samples were placed on a translation platform in petri dishes. The OCT camera was placed perpendicular to the samples and the plane of scanning was parallel to the marked anterior saw plane. Samples were placed in the same direction based on anatomical orientation, with respect to the scanning beam. The OCT system has a focal distance of 60 mm. After cross-sectional imaging, B-scans were composed from 300 A-lines. Volume-scans were 300 (x, length) by 300 (y, width) by 400 (z, depth) pixels (see Fig. 1(A)). Using 3-D visualization software (Amira, Visage Imaging, San Diego, CA, USA), the 300 B-scans were reconstructed into a three-dimensional dataset of 12.0 mm (x) by 12.0 mm (y) by 2.7 (z) mm, the latter dimension with an assumed refractive index of 1.4 for cartilage.

C. Histology

Following OCT scanning, samples were embedded in methyl methacrylate. Histological slides of 5 μm thickness were produced parallel to the marked ventral saw plane and stained with Hematoxylin and Eosin.

An expert pathologist (CDS) from the Department of Pathology at the Academic Medical Center evaluated the histological samples using light microscopy. In collaboration with the pathologist, high-resolution scans were made from the original histological slide of 5 μm using a slide scanner.

D. Selection of Matching OCT and Histology Images

A single histological slide clearly depicting the central osteochondral defect was chosen for each talus. 3-D OCT reconstructions assisted in identification of landmarks on the cartilage surface (like small tears and distinct surface topography) resembling the selected histological slide. From the 300 B-scan OCT dataset, utilizing the aforementioned landmarks, one matching OCT slide per talus was chosen for further analysis (see Fig. 2). Also, for attenuation analysis, one slide prior and one slide following the exact B-scan match were selected for analysis, resulting in 5 data points per talus.

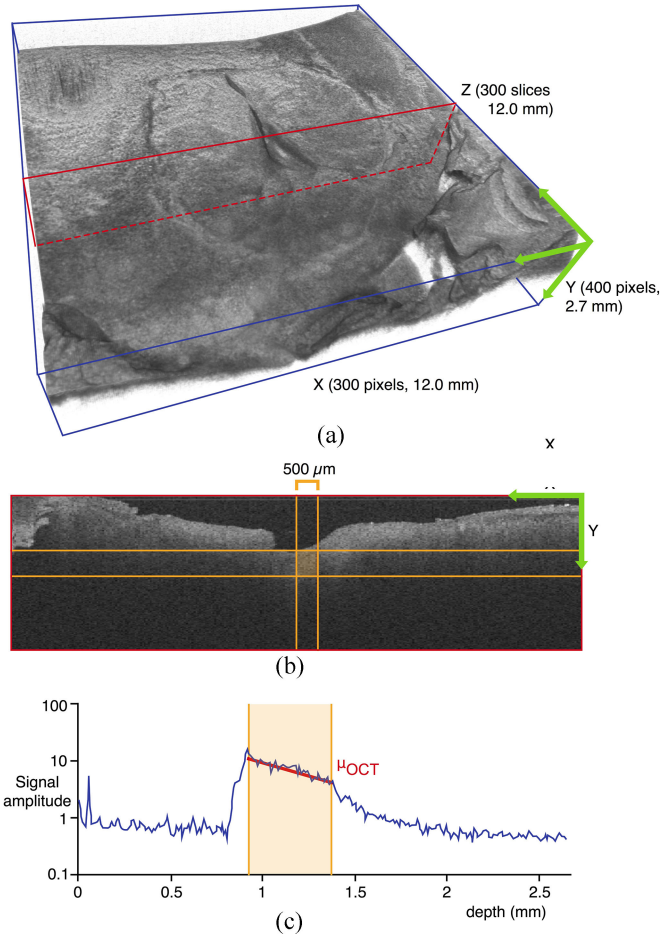

Fig 1. OCT data and Attenuation measurements. (A) 3-D volume reconstruction of an OCT dataset with dimensions in pixels and mm. (B) OCT slide taken from the 3-D dataset, position signified in red with ROI for attenuation measurement in orange. (C) OCT signal amplitude curve as a function of signal depth from the selected ROI (orange). μ_{OCT} is calculated by fitting the inclination of the OCT signal amplitude within the chosen ROI (red line) after calibration of depth-dependent signal loss due to the OCT system itself.

E. Light Attenuation Measurements

OCT signal attenuation measurements (μOCT) were performed using custom-made software as described before [19], utilizing the exponential decay of the OCT signal amplitude as a function of depth according to Lambert–Beer's Law

$$\left\langle i^2\left(z\right)\right\rangle = A exp\left(-2\mu_{\mathrm{OCT}}(z - z_0)\right). \tag{1}$$

Here, $\langle i^2(z)\rangle$ is the squared amplitude of the OCT signal, A is an amplitude used for scaling, z is depth coordinate and z_0 is the position of zero delay. Note that this model assumes

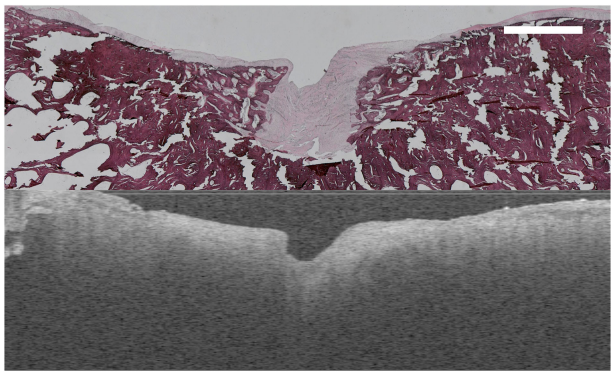

Fig 2. Histopathology slide (top) with matched OCT slide (bottom) showing healthy cartilage on both sides and repair tissue in the center of the image. Distinct surface topography and landmarks are identified in both slides. The scale bar represents 2 mm.

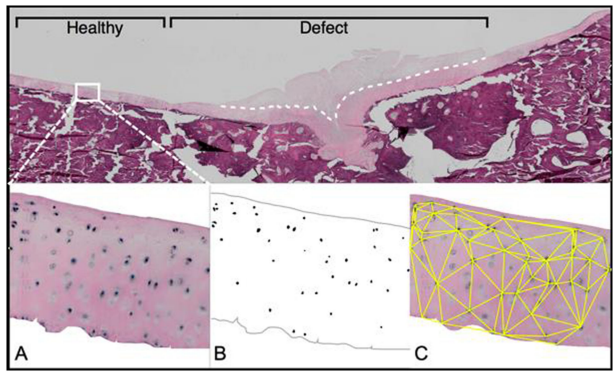

Fig. 3 Histology Measurements Exemplary measurement of the structural parameters *nucleus count per mm^2, nucleus size and inter-nucleus distance* using a custom made macro. In the histology slide, the white dashed line separates the upper- and lower layer. To illustrate the measurement, a small portion (white box) of the entire measured slice is shown (2A). After background subtraction and conversion to 8-bit binary, only nuclei remained for particle analysis (2B). After center of mass selection, Delaunay–Voronoi triangulation was performed with construction of lines (yellow) between the found nuclei to measure distances (2C). Local nuclear density is inversely proportional to the areas of the resulting triangles.

that system-induced signal loss with depth is accounted for through calibration as described earlier [20]. A-lines were averaged over a region of interest (ROI) of at least 500 μm (see Fig. 1(B)). Setup-specific calibration parameters such as the in-depth OCT sensitivity roll-off and the sample arm optics point spread function [21] were taken into account during attenuation measurements [22]. μ_{OCT} was measured for healthy cartilage (see Fig. 1(C)), repair tissue and subchondral bone. Also, guided by the OCT signal, two different layers could be discerned within repair tissue in a number of samples. ROI measurements were repeated five times in the same sample, choosing the same region in five adjacent slides for each measurement, producing a mean attenuation value for each specific region.

F. Polarization Microscopy

A light microscope with polarization filter (Universal Research, Carl Zeiss, Germany) was used to examine birefringence of light, revealing the presence and organization of collagen fibers.

G. Structural Histological Parameters

A custom-made macro for the open-source image-processing software Fiji [23] was used to quantify the number of nuclei per mm^2, nucleus size and the mean distance between nuclei from histologic slides (see Fig. 3). The macro was used to create a binary image, segmenting the nuclei from the original histological slide. For segmentation of nuclei, the same threshold was used for all slides to exclude "out of focus" nuclei. Nucleus size was analyzed using a built-in particle analysis function (see Fig. 3(B)).

Since the inter-nucleus distance can give insight into the degree of tissue organization, the mean distance between nearest-neighbor nuclei was measured; lines between adjacent nuclei were created by Delaunay–Voronoi triangulation on the histopathology image (see Fig. 3(C)). Distances between separate nuclei of more than 200 μm were excluded from analysis, since said lengths would span the entire thickness of the cartilage layer. The number of nuclei per mm^2 was calculated using the total number of nuclei from the particle analysis divided by the total area of the measured slide surface. In addition, the local nuclear density (per mm^2) was calculated per sample for both healthy cartilage and repair tissue, based on the Delaunay triangulation used for mean inter-nucleus distance measurements.

H. Statistics

Statistical analyses were performed using GraphPad Prism (version 5, GraphPad Software, Inc., La Jolla, CA, USA). Light attenuation measurements from healthy cartilage and repair tissue were checked for normality using d'Agostino Pearson's test. Values are given as mean $\pm$ standard deviation. Differences between measured parameters in healthy cartilage and repair tissue concerning light attenuation, number of nuclei, nucleus size and mean distance between nearest neighbor nuclei were tested using: 1. a paired T-test for data resembling a Gaussian distribution and 2. Wilcoxon's Signed Rank test was used for data in which no normal distribution was observed.

III. Results

A. OCT and Attenuation Measurements

On OCT images, the healthy cartilage tissue surface appeared smooth with a distinct region of high signal amplitude at the air-to-tissue interface (see Fig. 1(B)). The transitional zone from cartilage to subchondral bone was identified on all OCT scans. Repair tissue appeared fibrillated and irregular compared to the smooth surface in healthy cartilage. Also, relatively high signal intensities were found in deeper repair tissue zones compared to healthy cartilage signal intensities at the same depth.

Measured μOCT in healthy cartilage (9.7. $\pm$ 3.3 mm^{-1}) was higher compared to both repair tissue (3.1 $\pm$ 1.4 mm^{-1}; $p < 0.001$) and bone tissue (4.5 $\pm$ 0.5 mm^{-1}, $p = 0.001$). Measured μOCT in bone tissue was higher compared to repair tissue ($p = 0.007$). In eight of ten measured samples, a distinct upper and lower layer could be identified in the repair tissue region

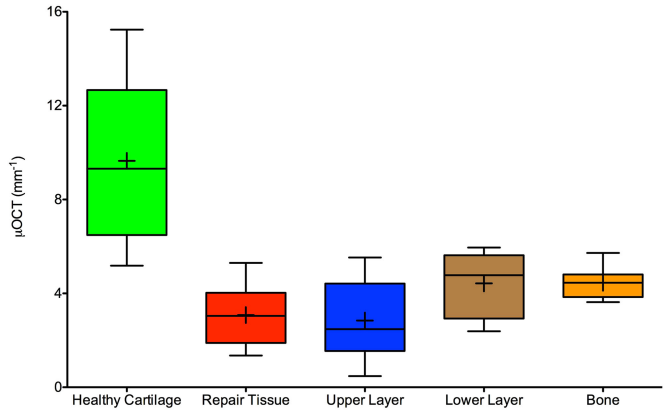

Fig. 4. Measured light attenuation (μ_{OCT}) per mm^{-1} in healthy cartilage, repair tissue, repair tissue upper- and lower layer and bone tissue. Box plots show median and quartiles, mean (+) and min and max (whiskers).

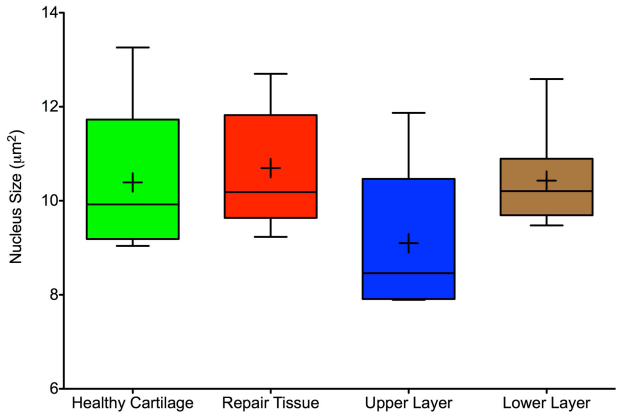

Fig. 5. Nucleus size in μm^2 in healthy cartilage, repair tissue, repair tissue upper- and lower layer. Box plots show median and quartiles, mean (+) and min and max (whiskers).

using OCT. A trend was observed in which light attenuation was lower in the upper layer (2.8 ± 1.7 mm^{-1}) compared to the lower layer (4.4 ± 1.4 mm^{-1}), although the difference was not significant. Compared to bone tissue, light attenuation was lower in the upper layer ($p = 0.022$), but no difference was observed when comparing bone tissue to the lower layer. Fig. 4 is a graphical representation of measured light attenuation in different tissue layers.

B. Histology and Structural Parameters

The areas defined as healthy cartilage had a smooth appearance and resembled hyaline (articular) cartilage (see Fig. 3(A)). The tissue displayed a high level of organization with nuclei organized in rows with seemingly regular intervals. The region of the former osteochondral defect (repair tissue) exhibited mainly fibro-cartilaginous tissue, consistent with damaged and subsequently repaired articular cartilage (see Fig. 3). Using light microscopy, in six of ten samples, an upper- and lower layer with structurally different appearances could be identified in the repair tissue zone. The upper layer of the repair tissue area appeared to exhibit loosely organized connective tissue with a low degree of organization and a lower nuclear density compared to the lower layer. The lower layer consisted of fibrous- and fibro-cartilaginous tissue with closer resemblance to osseous tissue than to hyaline cartilage.

Quantitative analysis of the nuclei present in the different tissue layers did not demonstrate a difference in nucleus size between any of the measured tissue types, although a trend was visible in which the upper layer contains slightly smaller nuclei (see Fig. 5).

As depicted in Fig. 6(A), a trend was observed in which the number of nuclei per mm^2 was higher in repair tissue compared to healthy cartilage. Notably, the range in nucleus count was much higher in repair tissue compared to healthy cartilage. The nucleus density in the repair tissue upper layer was lower compared to the lower layer ($p = 0.031$).

Fig. 6(B) demonstrates the local nucleus density per sample. We see a higher variation in nucleus density between repair tissue samples compared to healthy cartilage samples.

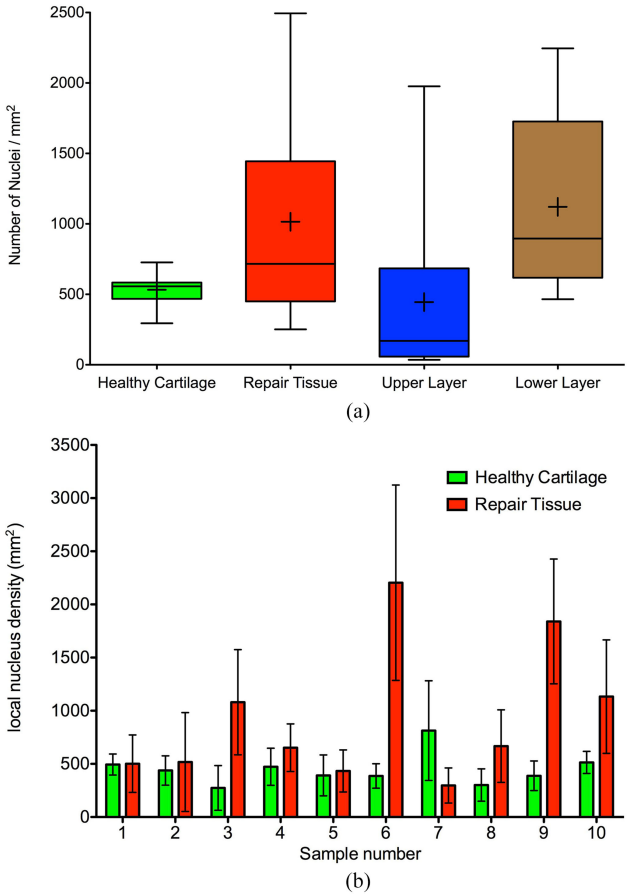

Fig. 6. (A) Nucleus count per mm^2 in healthy cartilage, repair tissue, repair tissue upper- and lower layer. Box plots show median and quartiles, mean (+) and min and max (whiskers). (B) Local nucleus count per mm^2, shown for each sample for healthy cartilage and repair tissue. Higher variation in local nuclear density was found in repair tissue.

The mean inter-nucleus distance was larger in healthy tissue compared to repair tissue ($p = 0.014$) and in the upper layer compared to the lower layer ($p = 0.031$), as depicted in Fig. 7. Again, the range in inter-nucleus distance was higher in repair tissue compared to healthy cartilage.

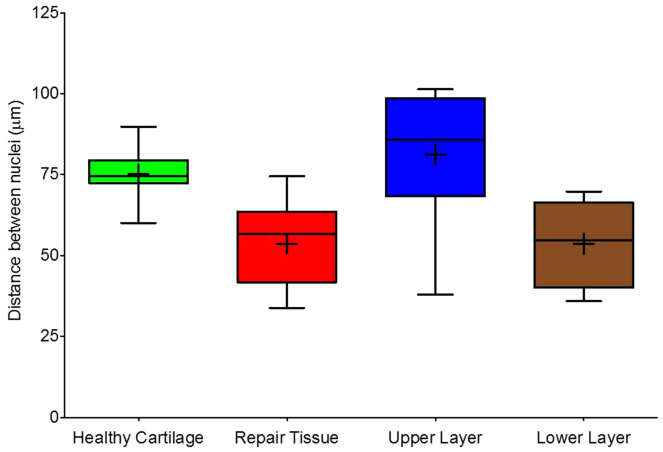

Fig. 7 Inter-nucleus distance. Measured distances in μm between nuclei in healthy cartilage, repair tissue, repair tissue upper- and lower layer. Box plots show median and quartiles, mean (+) and min and max (whiskers).

C. Polarization Microscopy

A polarized light microscope was used for qualitative assessment of collagen structures in different tissue types. In healthy cartilage, the presence of organized cartilage tissue was observed as areas with increased light intensity under polarized light illumination (see Fig. 8(A)).

When comparing both repair tissue and healthy cartilage in one frame and with the same light exposure, larger intensities were seen in healthy cartilage, especially relative to the adjacent repair tissue (see Fig. 8(B)), suggesting a higher collagen content and higher degree of organization in healthy cartilage. Moreover, polarization microscopy revealed evident differences between the repair tissue upper- and lower layer; lower layers exhibited thick collagen fibers with bright light intensities whereas upper layers showed almost no presence of fiber structures (see Fig. 8(C)). These observations could not be discerned using conventional light microscopy.

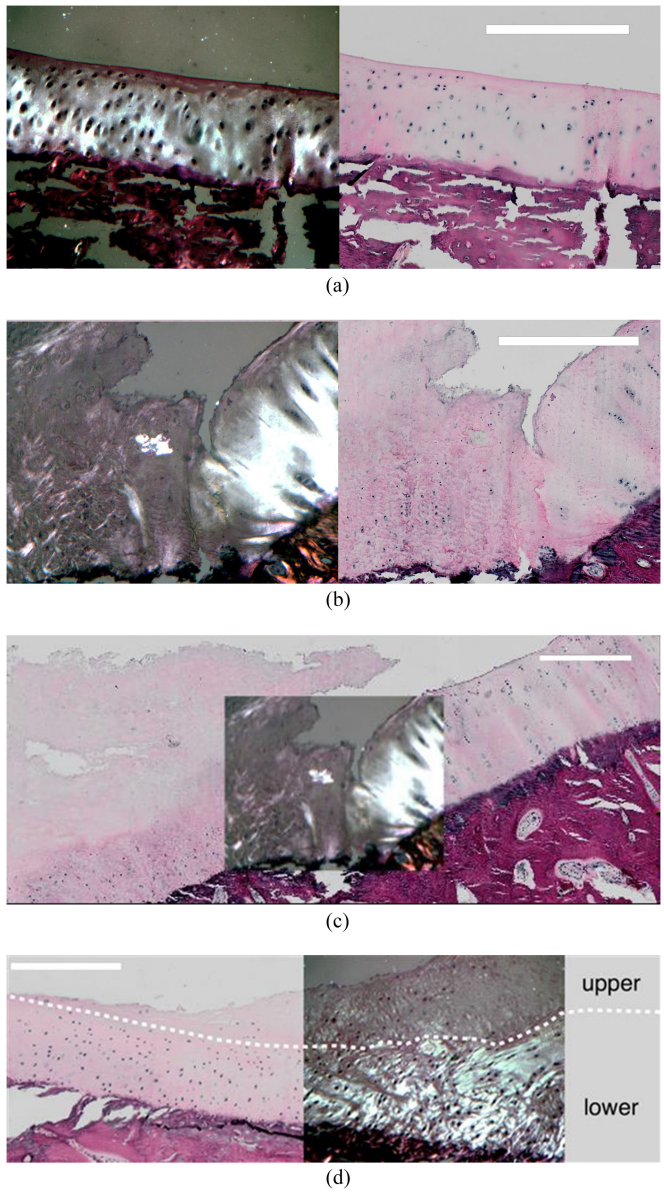

Fig. 8. (A) Histopathology slide of healthy cartilage under polarized light microscopy (left) and light microscopy (right). Cartilage nuclei are well organized in rows and a high intensity of the healthy cartilage layer is visible using polarized light microscopy. The white scale bar represents 300 μm. (B) Histopathology image of the transition zone between healthy cartilage and repair tissue with polarization microscopy overlay. Evident differences are visible between the bright healthy cartilage (right) and the relatively disorganized repair tissue (left). The white scale bar represents 300 μm. (C) Histopathology slide of repair tissue on light microscopy (left) and polarized light microscopy (right). The white scale bar represents 300 μm. On polarized light microscopy, distinct layers are discernible (upper- and lower layer divided by white dashed line in both images). The lower layer with thick collagen fibers is bright in contrast to the upper layer were these fibers are absent and less nuclei are present.

IV. Discussion

This study demonstrates a clear distinction between healthy cartilage, repair tissue structures and bone using OCT derived light attenuation in an *ex vivo* animal model, revealing a higher μOCT in healthy articular cartilage compared to repair tissue and bone. Moreover, this paper is the first to demonstrate quantitative assessment of optical properties in precisely matched slides with evident healthy and repair cartilage tissue and bone, within the same sample.

Previous studies showed that using μOCT, structural differences in different tissue types in the spine could be identified [11] and consequences of irradiation to the cartilage OCT signal could be illustrated [14]. Reports of the application of μOCT in imaging of articular cartilage have been sparse and hitherto, no underlying morphological explanations for measured differences in μOCT have been described [13], [15], [24]. However, quantification of evident differences in tissue structure will increase the value of OCT in clinical practice.

Two possible mechanisms for the difference in attenuation, described in, i.e., oncological tissue by previous research, were investigated [25]. We demonstrate that the significantly higher μOCT in healthy cartilage relative to repair tissue cannot be explained by quantitative morphological differences in terms of nucleus count, size and their mean inter-nucleus distance. Although our data show significant differences in μOCT, no

differences in nucleus size and nucleus count were observed between healthy cartilage and repair tissue.

Nonetheless, nuclei were spaced farther apart in healthy cartilage compared to repair tissue and a higher variation in local nucleus count was observed in repair tissue samples (see Fig. 6(B)). This leads to the hypothesis that differences in internal organization between healthy cartilage and repair tissue could be an explanation for μOCT differences.

Bear *et al.* found changes in backscattering- and attenuation coefficients where histology showed chondrocyte death and surface collagen matrix disruption. Also, it was shown that collagen fiber orientation causes distinct banding patterns when using a polarization sensitive OCT system [26], [27].

Li *et al.* showed a loss of the regular depth-resolved banding pattern in *in vivo* degenerative human knee cartilage [2]. In addition to aforementioned results, our qualitative assessment of polarization microscopy images indicate that collagen fiber content is substantially different between the measured tissue layers, as indicated in a previous study by Mansfield *et al*. [28].

The results suggest that in OCT imaging of articular cartilage and especially when assessing μOCT, the presence of collagen fibers and their orientation are main contributors to light scattering. In future studies, quantification of collagen fiber thickness and -orientation should be performed to confirm the results of this study, preferably in combination with polarization sensitive μOCT measurements.

Previous research has shown that OCT has the potential to detect cartilage damage associated with OA in an earlier stage compared to macroscopic inspection during arthroscopy [4], making OCT a relevant tool in clinical OA imaging. However, the results of this *ex vivo* animal study, in which clear differences in OCT signal attenuation were found between healthy cartilage and repair tissue, cannot be translated to clinical practice directly. Fixation of sample with formaldehyde, which is based on crosslinking of proteins, could be of influence on the optical properties of the tissue [29], [30]. To further assess the role of attenuation measurements as a standalone diagnostic tool in clinical practice, additional experiments have to be performed, preferably on *ex vivo* or *in vivo* human tissue. Also, recent research has demonstrated that additional parameters in 3-D cartilage OCT assessment, like layer thickness, tissue roughness or optical irregularity may be useful in diagnostics of cartilage degeneration [31].

This study highlights the value of OCT in detection of subtle cartilage pathology. This is of clinical importance since detection of cartilage damage in early OA might be reversible [3]. Therefore, OCT continues to be a very promising technique in quantitative imaging of early OA in small joints.

V. Conclusion

We present quantitative cartilage imaging by means of μOCT, tested in a controlled setting, assessing five distinct tissue layers within the same sample. This study reveals that μOCT measurements can distinguish between healthy cartilage and repair tissue and bone in an *ex vivo* animal model, as confirmed with histopathology. Furthermore, results suggest that differences in the highly scattering character of articular cartilage relative to repair tissue may be caused by the degree of collagen content rather than differences in nucleus count, size and inter-nucleus distance.

Since the use of fiber optic OCT for intra-articular cartilage imaging has already been demonstrated, these results greatly increase the value of cartilage OCT in detection of early cartilage pathology and provide understanding in additional quantification of the OCT signal in clinical diagnostics.

Acknowledgment

The authors would like to thank J. Bras, O. de Boer, and H. van Veen for their contribution to this study.

References

[1] P. Cernohorsky *et al.*, "In-situ imaging of articular cartilage of the first carpometacarpal joint using co-registered optical coherence tomography and computed tomography.," *J. Biomed. Opt.*, vol. 17, no. 6, p. 060501, Jun. 2012.

[2] X. Li *et al.*, "High-resolution optical coherence tomographic imaging of osteoarthritic cartilage during open knee surgery.," *Arthritis Res. Ther.*, vol. 7, no. 2, pp. R318–R323, 2005.

[3] C. R. Chu, N. J. Izzo, J. J. Irrgang, M. Ferretti, and R. K. Studer, "Clinical diagnosis of potentially treatable early articular cartilage degeneration using optical coherence tomography," *J. Biomed. Opt.*, vol. 12, no. 5, p. 051703, Aug. 2007.

[4] K. Zheng, S. D. Martin, C. H. Rashidifard, B. Liu, and M. E. Brezinski, "In vivo micron-scale arthroscopic imaging of human knee osteoarthritis with optical coherence tomography: Comparison with magnetic resonance imaging and arthroscopy," *Amer. J. Orthopedics*, vol. 39, no. 3, pp. 122–125, Mar. 2010.

[5] J. M. Herrmann *et al.*, "High resolution imaging of normal and osteoarthritic cartilage with optical coherence tomography," *J. Rheumatol.*, vol. 26, no. 3, pp. 627–635, Mar. 1999.

[6] S.-K. Han, S. Federico, M. Epstein, and W. Herzog, "An articular cartilage contact model based on real surface geometry," *J. Biomech.*, vol. 38, no. 1, pp. 179–184, Jan. 2005.

[7] C. R. Chu *et al.*, "Arthroscopic microscopy of articular cartilage using optical coherence tomography," *Amer. J. Sports Med.*, vol. 32, no. 3, pp. 699–709, Mar. 2004.

[8] N. C. R. Te Moller *et al.*, "Arthroscopic optical coherence tomography provides detailed information on articular cartilage lesions in horses," *Veterinary J.*, vol. 197, pp. 589–595, Jun. 2013.

[9] N. A. Patel, J. Zoeller, D. L. Stamper, J. G. Fujimoto, and M. E. Brezinski, "Monitoring osteoarthritis in the rat model using optical coherence tomography," *IEEE Trans. Med. Imag.*, vol. 24, no. 2, pp. 155–159, Feb. 2005.

[10] M. T. J. Bus *et al.*, "Volumetric in vivo visualization of upper urinary tract tumors using optical coherence tomography: A pilot study," *J. Urol.*, vol. 190, no. 6, pp. 2236–2242, Dec. 2013.

[11] K. Beaudette *et al.*, "Optical coherence tomography for the identification of musculoskeletal structures of the spine: A pilot study," *Biomed. Opt. Exp.*, vol. 3, no. 3, pp. 533–542, Mar. 2012.

[12] R. R. Wessels *et al.*, "Optical coherence tomography in vulvar intraepithelial neoplasia," *J. Biomed. Opt.*, vol. 17, no. 11, pp. 116022–116022, Oct. 2012.

[13] D. M. Bear *et al.*, "Optical coherence tomography detection of subclinical traumatic cartilage injury," *J. Orthopedics Trauma*, vol. 24, no. 9, pp. 577–582, Sep. 2010.

[14] A. C. Martinho, Jr., et al., "Dependence of optical attenuation coefficient and mechanical tension of irradiated human cartilage measured by optical coherence tomography," *Cell Tissue Bank*, vol. 15, pp. 337–343, Jul. 2013.

[15] P. Cernohorsky *et al.*, "Comparison of optical coherence tomography and histopathology in quantitative assessment of goat talus articular cartilage," *Acta Orthopedics*, vol. 86, no. 2, pp. 257–263, Apr. 2015.

[16] J. R. Mourant *et al.*, "Light scattering from cells: The contribution of the nucleus and the effects of proliferative status," *J. Biomed. Opt.*, vol. 5, no. 2, pp. 131–137, Apr. 2000.

[17] J. D. Wilson, W. J. Cottrell, and T. H. Foster, "Index-of-refraction-dependent subcellular light scattering observed with organelle-specific dyes," *J. Biomed. Opt.*, vol. 12, no. 1, p. 014010, Jan. 2007.
[18] A. C. Kok *et al.*, "No effect of hole geometry in microfracture for talar osteochondral defects," *Clin. Orthopedics Related Res.*, vol. 471, no. 11, pp. 3653–3662, Nov. 2013.
[19] D. Faber, F. van der Meer, M. Aalders, and T. van Leeuwen, "Quantitative measurement of attenuation coefficients of weakly scattering media using optical coherence tomography," *Opt. Exp.*, vol. 12, no. 19, pp. 4353–4365, Sep. 2004.
[20] B. G. Muller *et al.*, "Prostate cancer diagnosis: The feasibility of needle-based optical coherence tomography," *J. Med. Imag.*, vol. 2, no. 3, p. 037501, Jul. 2015.
[21] T. G. van Leeuwen, D. J. Faber, and M. C. Aalders, "Measurement of the axial point spread function in scattering media using single-mode fiber-based optical coherence tomography," *IEEE J. Sel. Topics Quantum Electron.*, vol. 9, no. 2, pp. 227–233, Mar. 2003.
[22] D. M. de Bruin *et al.*, "Optical phantoms of varying geometry based on thin building blocks with controlled optical properties," *J. Biomed. Opt.*, vol. 15, no. 2, p. 025001, Feb. 2010.
[23] J. Schindelin *et al.*, "Fiji: An open-source platform for biological-image analysis," *Nature Methods*, vol. 9, no. 7, pp. 676–682, Jul. 2012.
[24] J.-J. Shyu *et al.*, "Diagnosis of articular cartilage damage by polarization sensitive optical coherence tomography and the extracted optical properties," *Prog. Electromagn. Res.*, vol. 91, pp. 365–376, 2009.
[25] O. C. Marina, C. K. Sanders, and J. R. Mourant, "Correlating light scattering with internal cellular structures," *Biomed. Opt. Exp.*, vol. 3, no. 2, pp. 296–312, Feb. 2012.
[26] W. Drexler *et al.*, "Correlation of collagen organization with polarization sensitive imaging of in vitro cartilage: Implications for osteoarthritis," *J. Rheumatol.*, vol. 28, no. 6, pp. 1311–1318, Jun. 2001.
[27] S. J. Matcher, "A review of some recent developments in polarization-sensitive optical imaging techniques for the study of articular cartilage," *J. Appl. Phys.*, vol. 105, no. 10, p. 102041, 2009.
[28] J. C. Mansfield, C. P. Winlove, J. Moger, and S. J. Matcher, "Collagen fiber arrangement in normal and diseased cartilage studied by polarization sensitive nonlinear microscopy," *J. Biomed. Opt.*, vol. 13, no. 4, p. 044020, Jul. 2008.
[29] R. Thavarajah, V. K. Mudimbaimannar, J. Elizabeth, U. K. Rao, and K. Ranganathan, "Chemical and physical basics of routine formaldehyde fixation," *J. Oral Maxillofacial Pathol.*, vol. 16, no. 3, pp. 400–405, Sep. 2012.
[30] P.-L. Hsiung, P. R. Nambiar, and J. G. Fujimoto, "Effect of tissue preservation on imaging using ultrahigh resolution optical coherence tomography," *J. Biomed. Opt.*, vol. 10, no. 6, p. 064033, Nov. 2005.
[31] N. Brill *et al.*, "3D Human cartilage surface characterization by optical coherence tomography," *Phys. Med. Biol.*, vol. 60, no. 19, pp. 7747–7762, Sep. 2015.

Paul Cernohorsky received the medical degree from the faculty of Medical Sciences of the University of Groningen in 2012. He is currently working toward the Ph.D. degree at the Academic Medical Center, University of Amsterdam, The Netherlands. He is with the Department of Biomedical Engineering and Physics and the Department of Plastic, Reconstructive, and Hand Surgery at the Academic Medical Center.

Sanne M. Jansen is currently working toward the Ph.D. degree at the Academic Medical Center, University of Amsterdam, The Netherlands. She is with the Department of Biomedical Engineering and Physics and the Department of Plastic, Reconstructive, and Hand Surgery at the Academic Medical Center, involved in optical imaging techniques in clinical diagnostics.

Daniel M. de Bruin is currently a Staff Member at the Department of Urology, University of Amsterdam, Amsterdam, The Netherlands, where he is also a Research Associate at the Department of Biomedical Engineering and Physics. In this combined position, he initiates new research lines which will ultimately result in a minimal invasive optical diagnosis and in novel focal treatment of (epithelial) cancers.

Edwin van der Pol is currently a Postdoctoral Researcher at both the Department of Biomedical Engineering and Physics and the Laboratory of Experimental Clinical Chemistry in the Academic Medical Center, University of Amsterdam, Amsterdam, The Netherlands. His research interests include the detection of exosomes, microvesicles, and other extracellular vesicles as biomarkers for disease.

Cemile D. Savci-Heijink received the Medical degree in Ankara, Turkey. She received the residency training in anatomical pathology at the Marmara University, Istanbul, Turkey, followed by additional training at Mayo Clinic, Rochester, NY, USA. She is currently a Consultant Pathologist at the Academic Medical Center, University of Amsterdam, Amsterdam, The Netherlands. Her research interests include urological pathology and bone and soft tissue pathology.

Simon D. Strackee is a Plastic and Reconstructive Hand Surgeon at the Academic Medical Center, University of Amsterdam, Amsterdam, The Netherlands. His research interests include free flap reconstruction and hand surgery.

Dirk J. Faber is currently an Associate Professor at the Academic Medical Center, University of Amsterdam, Amsterdam, The Netherlands, where he is with the Biophotonics Group of the Department of Biomedical Engineering and Physics. His research interests include physical understanding of the optical signals, novel instrumentation, novel contrast mechanisms, and clinical application.

Ton G. van Leeuwen is a Professor of biomedical physics and also the Chairman of the new Department of Biomedical Engineering and Physics, Academic Medical Center, University of Amsterdam, Amsterdam, The Netherlands, where he is involved in the fusion of engineering and physics with life sciences and clinical medicine, thereby providing further understanding of pathological processes and contributing to development and improvement of diagnostic and therapeutic tools.